Mid-Infrared Astronomy with NGST

Ewine F. van Dishoeck

Leiden Observatory, P.O. Box 9513, NL–2300 RA Leiden, The Netherlands

Abstract. The mid-infrared wavelength range from 5–30 μm is a key region for studying the origin and evolution of galaxies, stars and planetary systems. NGST can address and resolve outstanding scientific questions in this area because of its orders of magnitude higher sensitivity and spatial resolution compared with existing or planned facilities. An overview of mid-infrared continuum and line (atomic, molecular, solid-state) radiation is given and the uniqueness of mid-infrared features compared with those at other wavelengths (near-IR, millimeter) is stressed. The scientific prospects for NGST are illustrated using recent data from the Infrared Space Observatory on a variety of topics ranging from starburst galaxies in the early universe to the evolution of organic and solid-state matter in planet-forming disks around young stars in the solar neighborhood.

1. Introduction

The formation of stars and planetary systems takes place deep inside clouds of gas and dust, often obscured by hundreds of magnitudes of extinction. At high redshifts, the assembly of galaxies through the merging of smaller units is accompanied by large amounts of dust. Indeed, soon after the first vigorous burst of star formation, galaxies in the early universe become obscured by their own dust. In order to penetrate these dusty regions, observations at long wavelengths are essential. A mid-infrared camera and spectrometer on NGST would be an extremely powerful and unique tool to study the physical and chemical processes associated with the origin of galaxies, stars and planets, and an essential complement to near-infrared and millimeter observations.

NGST will have unprecedented sensitivity and spatial resolution at mid-infrared wavelengths. Figure 1 illustrates the expected imaging sensitivity compared with other facilities. NGST will be three orders of magnitude more sensitive than any ground-based telescope in the 5–30 μm range, part of which will be completely blocked by atmospheric features from the ground. Compared with SIRTF, NGST will have more than an order of magnitude increase in sensitivity and spatial resolution. Moreover, SIRTF will have only very low resolution spectroscopy R=$\lambda/\Delta\lambda$=50–100 in the important 5–10 μm range, and R=600 in the 10–38 μm range. As will be shown below, such low resolving powers are insufficient for many key scientific programs. Thus, NGST has the potential to perform unique science in a poorly explored wavelength range, increasingly substantially the NGST discovery space.

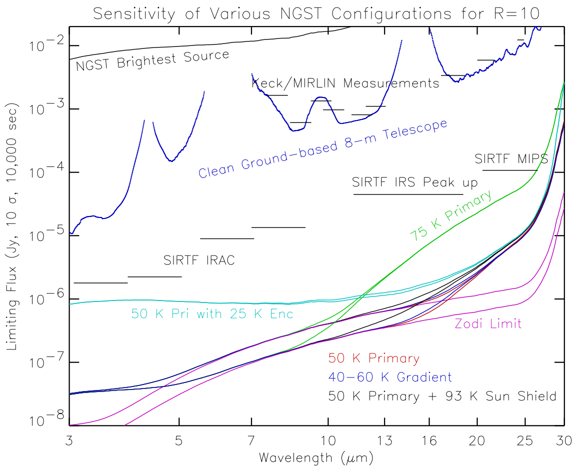

Figure 1. Imaging sensitivity at R=10 of NGST (dark solid lines) compared with ground-based telescopes and SIRTF (Serabyn et al. 1999).

In this brief paper, an overview of the basic processes and spectral features at mid-infrared wavelengths will be given, followed by a few scientific highlights based on recent results from the Infrared Space Observatory (ISO). The general mid-infrared science case for NGST has been well-described in the ISIM studies by Serabyn et al. (1999) and Wright et al. (1999), whereas an overview of recent ISO results can be found in the proceedings of the conference "The Universe as seen by ISO" (ESA SP-427, ed. P. Cox and M.F. Kessler).

2. Mid-infrared processes and features

In the local universe, the continuum at mid-infrared wavelengths is dominated by thermal emission from warm dust with $T_{\rm dust} \approx 100-300$ K, such as found in star-forming regions and around late-type stars (red giants, AGB and post-AGB stars). The ultraviolet and optical radiation from these stars is absorbed by the dust and re-radiated at longer wavelengths. In addition, thermal emission from the atmospheres of cool stars (K, M, L, ...), from brown dwarfs with effective temperatures $T_{\rm eff} \approx 1000$ K, and from solar-system objects such as comets and Kuiper-Belt objects is significant at mid-infrared wavelengths. Any non-thermal (synchrotron) contribution is generally small. In addition to their own intrinsic interest, observations at longer wavelengths are needed to distinguish the contributions of various processes to broad-band colors at near-infrared wavelengths.

The mid-infrared is rich in spectral features, many of which are unique for this wavelength range. These features are illustrated in the ISO Short Wavelength Spectrometer (SWS) spectrum of one of the brightest mid-infrared sources in the sky, the Orion-KL region (Figure 2) and are summarized in Table 1.

Atomic and ionic fine-structure lines: Fine-structure transitions within the lowest electronic term of most astrophysically relevant atoms and ions occur in the 5–30 μm range. Important examples are the [Ar II] 7.0, [Ne II] 12.8, [Ne V] 14.3,

Table 1. Some important spectral features in the mid-infrared

Category	λ (μm)	Species/ Line	Diagnostic[a]
Ions	7.0	[Ar II]	Radiation field,
	9.0	[Ar III]	Shocks,
	10.5	[S IV]	Spectral index,
	12.8	[Ne II]	Density,
	14.3	[Ne V]	Metallicity
	15.6	[Ne III]	
	18.7	[S III]	
	25.2	[S I]	
	25.9	[O IV]	
PAHs	3.3		Carbonaceous material,
	6.2		UV radiation,
	7.7		Redshift obscured galaxies
	8.6		
	11.3		
	12.7		
	14.2		
	16.2		
Silicates	9.7		Bulk of dust
(Amorphous)	18.0		
Silicates	10.0	Mg_2SiO_4	Mineralogy,
(Crystalline)	11.3		Heating events,
	16.3		Solar system connection
	19.5		(meteorites, IDP's, ...),
	23.5		Interpretation of SED
	27.5		
	33.5		
	18.5	$(Mg,Fe)SiO_3$	
	21.5		
	24.5		
Oxides	11.6	Al_2O_3	
	23	FeO	
Ices	6.0	H_2O	Volatile solid material,
	6.8	CH_3OH	Building blocks complex organics,
	7.7	CH_4	Solar system connection
	9.7	CH_3OH	(comets, KBOs),
	9.7	NH_3	Thermal history
	15.2	CO_2	
H_2	6.9	$7\rightarrow5$	Mass + temperature of bulk of warm gas,
	8.0	$6\rightarrow4$	Photon- vs shock-heating
	9.7	$5\rightarrow3$	
	12.2	$4\rightarrow2$	
	17.0	$3\rightarrow1$	
	28.2	$2\rightarrow0$	
HD	19.4	$6\rightarrow5$	[D]/[H]
	23.0	$5\rightarrow4$	
	28.5	$4\rightarrow3$	
Gas-phase	6.0	H_2O	Temperature + density structure,
Molecules	7.7	CH_4	Building blocks complex organics
	13.7	C_2H_2	
	14.0	HCN	
	15.0	CO_2	

[a]Diagnostic properties of category of species; individual species or lines probe a subset of these properties.

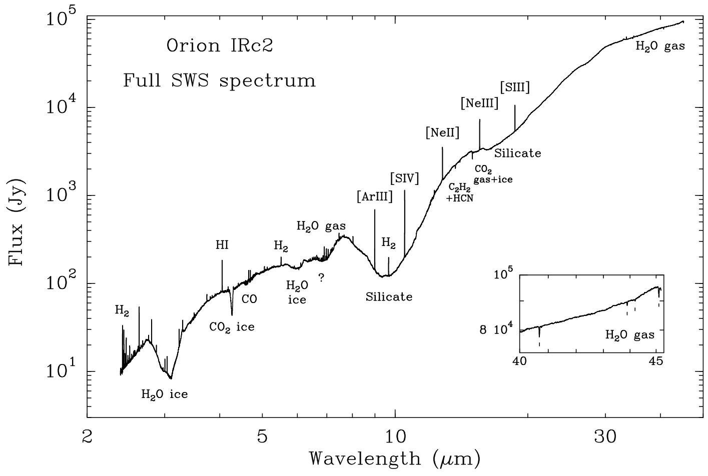

Figure 2. Complete ISO–SWS grating spectrum centered at Orion IRc2 at a resolving power R=1300–2500. The principal absorption and emission features are indicated. The ISO-SWS beam ranges from $14'' \times 20''$ to $20'' \times 27''$, and encompasses both the IRc2 and BN sources (van Dishoeck et al. 1998).

[Ne III] 15.6, [S I] 25.2, and [O IV] 25.9 μm lines, but even higher ionization stages ("coronal" lines) can be observed. These features are used as probes of the ionizing source, especially the hardness of the radiation field (e.g., starbursts vs. AGN), and as diagnostics of heating mechanisms, in particular shock– vs. photon-heating. The strongest lines can also be used to trace the kinematics of gas in obscured regions.

PAHs: The C-C and C-H stretching and bending modes of polycyclic aromatic hydrocarbons (PAHs) at 6.2, 7.7, 8.6, 11.3, ... μm often dominate the mid-infrared emission. More recently, new features at 16.2 μm and longer wavelengths have been found in ISO-SWS spectra, which contain important diagnostic information about the type of species involved (Tielens et al. 1999). Significant variations of factors of five or more can occur in the ratios of various bands, e.g. 8.6/7.7 and 11.3/7.7 μm, which appear related to differences in the ionization and hydrogenation state of the carriers. Since they are so prominent, the PAH features dominate the energy budget in this wavelength range, and are also the best redshift indicators for distant, obscured galaxies.

H_2 and HD pure rotational lines: The lowest transitions of the most abundant molecule in the universe, H_2, occur at mid-infrared wavelengths. Compared with a heavy molecule like CO, the energy levels of H_2 have a much wider spacing (see Figure 3). Moreover, H_2 has no dipole moment and can therefore only radiate through the much weaker quadrupole transitions. The fundamental $J = 2-0$ S(0) line of para-H_2 occurs at 28.22 μm, whereas the next transition, the $J = 3-1$ S(1) line of ortho-H_2, lies at 17.03 μm. Since the populations of these levels are thermalized under most conditions, the S(0) and S(1) lines provide a direct measure of the mass and temperature of the *bulk* of warm molecular gas at $T = 50-200$ K. In contrast, the higher pure rotational lines,

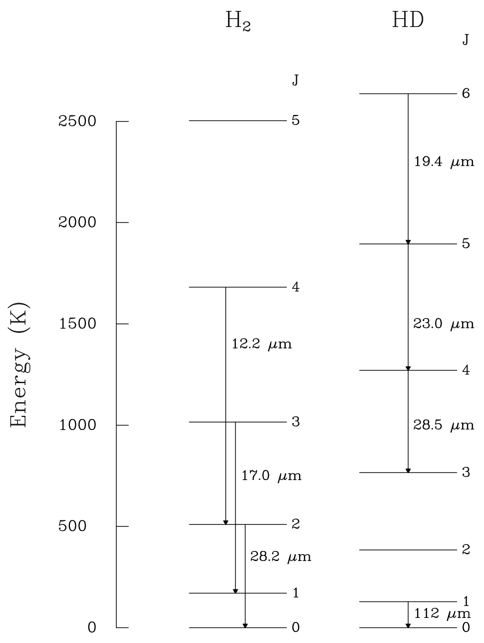

Figure 3. Energy level diagram of the H_2 and HD molecules, illustrating the fundamental pure rotational transitions.

as well as the vibration-rotation lines at 2 μm, probe only the small fraction (< 1 %) of photon- or shock-heated gas in the beam (Draine & Bertoldi 1999, Wright 2000). The heavier isotope, HD, has a small dipole moment and its lowest J=1–0 line at 112 μm has been detected with the ISO-LWS (Wright et al. 1999). The higher J=4–3, 5–4 and 6–5 lines occur at 28.5, 23.0 and 19.4 μm. The latter line has been observed by Bertoldi et al. (1999) in the Orion shock and can, in combination with H_2 data, be used to determine the [D]/[H] ratio in star-forming regions, providing constraints on the amount of astration since the production of deuterium in the Big Bang. Such data would be complementary to ultraviolet absorption line observations with FUSE, which can only probe the local diffuse interstellar medium within 2 kpc from the Sun.

Solid-state vibrational bands: The characteristic vibrational bands of ices, silicates and oxides occur uniquely at mid-infrared wavelengths. Solid-state species can be distinguished from gas-phase molecules because their bands lack the characteristic ro-vibrational structure and are broadened (see Figure 4). The Si–O stretching and bending bands of amorphous silicates at 9.7 and 18 μm are well known, but features of crystalline silicates and oxides at longer wavelengths have been discovered only recently by the ISO–SWS in circumstellar matter around young and old stars (Waters et al. 1996, Waelkens et al. 1996). Complete wavelength coverage of the mid-infrared wavelength range allows an inventory of these species to be made, whereas their lineshapes and abundances are sensitive diagnostics of heating events and the temperature history of the region (see §4.2, §5).

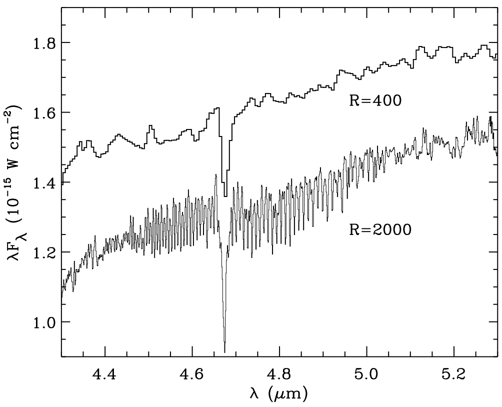

Figure 4. ISO-SWS spectra toward the young stellar object Elias 29 in the region of the CO vibrational band at R=400 and 2000. At R=400, solid CO at 4.67 μm is detected, but the intrinsically much narrower lines of gas-phase CO between 4.5 and 5 μm only become visible at R=2000, illustrating the need for medium resolution spectroscopy (Boogert 1999).

Gas-phase vibrational bands: Fundamental vibrational transitions of important organic molecules such as CH_4, C_2H_2, HCN and CO_2 occur at 7.7, 13.7, 14.0 and 15.0 μm, whereas the bending mode of H_2O lies at 6.0 μm. Symmetric molecules like CH_4 and C_2H_2 have no dipole moment and can therefore not be observed through rotational transitions at millimeter wavelengths. Moreover, CO_2 and H_2O are so abundant in the Earth's atmosphere that they can only be observed from space. In addition to its importance in organic chemistry, CH_4 is also an excellent diagnostic of the atmospheres of brown dwarfs and extrasolar giant planets (Burrows et al. 1997).

Red-shifted bands: For objects at high redshifts, the features discussed above are shifted further into the mid-infrared wavelength range, and the potential of NGST to detect these lines in distant galaxies is mostly limited by the available wavelength range rather than the sensitivity. For example, the strong [Ne II] 12.3 μm line shifts beyond 30 μm at $z > 1.4$, whereas the 6.2 μm PAH band shifts out of the range at $z > 3.8$. Strong near-infrared bands such as Br γ can be searched up to $z \approx 12$, whereas Hα enters the mid-infrared range at $z > 6.6$.

Need for medium spectral resolution: A resolving power $R = \lambda/\Delta\lambda \approx 2000-3000$ is required for several reasons. First, as illustrated in Figure 4, solid-state features are visible at R=400, but the ro-vibrational bands of gas-phase CO become apparent only at $R \geq 2000$. Second, sub-structure in the solid-state bands is an important diagnostic tool and requires $R \approx$1500 (§4.2, §5). Also, many solid-state bands overlap at longer wavelengths and cannot be distinguished at $R < 1500$. Third, detection of the intrinsically weak and narrow H_2 S(0) and S(1) lines on top of strong mid-infrared dust continuum emission requires $R \approx 3000$ to get sufficient line/continuum ratio. Finally, the kinematics of galaxies (e.g., stellar mass determinations from the red-shifted CO 2.3 μm band) and out-

Table 2. Comparison between 8-m NGST mid-infrared and ALMA

NGST	ALMA
5–30 μm	300–3000 μm
$0.16''$–$0.94''$	$0.05''$–$5''$
Warm dust (100–300 K)	Cold dust (10–100 K)
Many ionic lines	[C I], red-shifted [C II]
Ices, silicates	...
PAHs	...
H_2	CO
CH_4, C_2H_2, CO_2, ...	Myriad of (low-abundance) molecules
R$\approx 1500 - 3000$	R$> 10^6$

flows from protostars require velocity resolutions of 100–300 km s^{-1} or better, corresponding to $R \approx 1000 - 3000$.

Long-wavelength limit: As Table 1 illustrates, important features occur throughout the mid-infrared wavelength range. The lowest H_2 S(0) line sets a natural limit at 28.22 μm, but the presence of a strong crystalline silicate feature at 33.5 μm (cf. Figure 13) argues for extension up to 35 μm. Observations of red-shifted PAH features and ionic lines also warrant extension to longer wavelengths.

Comparison with ALMA: A mid-infrared instrument on NGST is an ideal complement to the Atacama Large Millimeter Array (ALMA), planned to be fully operational around the same time as NGST. The two facilities have comparable spatial resolution, but probe different physical regimes (see Table 2). For example, in circumstellar disks NGST will probe the warm inner planet-forming region whereas ALMA is more sensitive to the colder outer part. Moreover, the mid-infrared is unique in ionic lines and in solid-state/PAH features.

3. Distant obscured star formation

3.1. High-redshift galaxies

Unravelling the star- and galaxy formation history of the universe is the major science driver of NGST. Recent ISOCAM mid-infrared and SCUBA submillimeter observations suggest that star formation rates derived from optical data may be strongly underestimated (e.g., Elbaz et al. 1999, Smail et al. 1997, Hughes et al. 1998, Blain et al. 1999). Specifically, the deepest 15 μm surveys to date of lensed galaxy clusters such as Abell 2390 (Figure 5) show clear evidence for an increase in the number counts at the faint end, indicative of a new, dusty population of galaxies at $z > 0.2$ (Figure 6). These galaxies can make a substantial contribution to the overall energy budget and are responsible for a significant part of the mid-infrared background radiation. Since their optical colors are similar, mid-infrared observations provide the only method to distinguish this population. NGST will be able to push these surveys three orders of magnitude deeper and detect young galaxies out to redshifts of 10, determining their luminosity function (Serabyn et al. 1999). Typical source counts will be $\sim 10^6$ objects per square degree at the 1 μJy level, with a significant fraction of objects at $z > 1$. The mid-infrared range will be particularly well suited to trace the first quasars in the universe (Haiman & Loeb 1998). Compared with

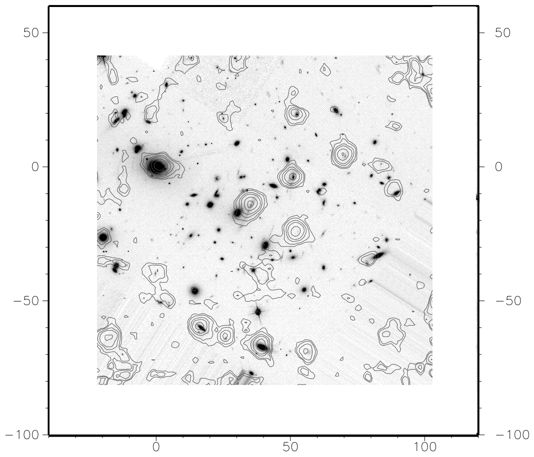

Figure 5. ISOCAM 15 μm image (contours) of the cluster Abell 2390 superposed on an HST I-band image. The scale is in arcsec. Several objects are detected with extremely red colors and very faint or absent I-band fluxes. The implied photometric redshifts of these red objects are greater than 3 (Metcalfe et al. 1999, Altieri et al. 1999).

SIRTF, NGST does not suffer from confusion because of its much higher spatial resolution ($0.9''$ vs. $9''$ at 28 μm). NGST will be important to follow-up and resolve the millions of sources that will be detected in the coming decade with SIRTF and with large bolometer arrays on ground-based single-dish submillimeter telescopes.

Mid-infrared observations of red-shifted 2 μm emission are also essential to reveal any old stellar population with mean age >50–100 Myr, which would be indicative of a previous episode of star formation, for example in the bulges of galaxies. Indeed, mid-infrared data are very important to resolve the ambiguity in the ages and amount of dust derived from near-infrared colors. The total mass in early spheroids can be measured through the velocity dispersions of the red-shifted CO 2.3 μm bands.

3.2. Probing the "active" universe

In nearby, spatially-resolved galaxies, ISOCAM images have revealed that most of the mid-infrared luminosity is located in a few "hot spots" with luminosities $> 10^{11}$ $L_\odot$ which are not seen at VIS/near-IR wavelengths and which are often offset from the nucleus. Excellent examples are provided by the comparison of visible and mid-infrared images of the Antennae galaxies (Vigroux et al. 1996) and the Mrk 171/Abell 299 system (Laurent et al. 1999). The mid-infrared data are essential to determine the true star formation rates of these objects.

More importantly, mid-infrared spectra provide insight into the physical processes occurring in these forming galaxies through a wide range of diagnostic probes. Indeed, NGST will be particularly powerful to probe the "active" universe between $z = 1 - 5$ when the star-formation rate may have peaked. The power of mid-infrared spectroscopy to disentangle the contributions from AGN and starbursts to the total luminosity has been illustrated in a series of recent

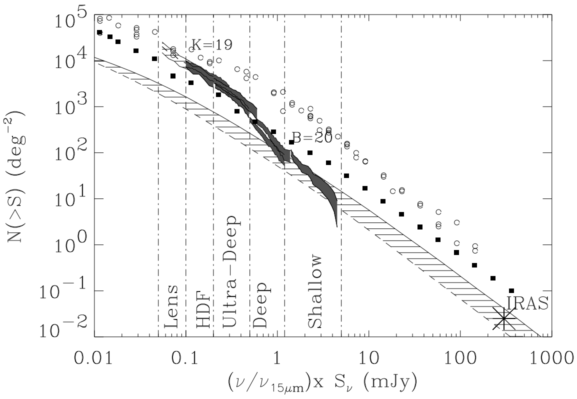

Figure 6. ISOCAM 15 μm integral counts, i.e. number of galaxies N detected above a flux S (mJy), with 68% confidence contours (dark band). The hatched area represents the range of expectations from models assuming no evolution and normalized to the IRAS 12 μm local luminosity function. The ISOCAM 15 μm results show up to a factor of 10 excess compared with the no-evolution models at the faintest measured fluxes (Elbaz et al. 1999).

papers (e.g., Genzel et al. 1998, Lutz et al. 1998). Spectra of starburst galaxies show strong PAH emission and lines from low ionization stages, whereas spectra of dust-enshrouded AGN lack the PAH features but show lines from high ionization stages such as [O IV] and [Ne V]. Diagrams of the [O IV]/[Ne II] ratio vs. strength of the 7.7 μm PAH feature can be used to infer the relative contributions from the two components on a global scale (Figure 7).

ISO was able to observe spectroscopic features up to $z \approx 0.1$ in luminous galaxies with $L > 5 \times 10^{11}$ $L_\odot$. SIRTF will be able to detect them up to $z \approx 1$, and perhaps more distant for the most powerful ULIRGS. In contrast, NGST should be able to detect these lines for more normal L_*- or Milky-Way type galaxies up to $z \approx 3$, when the features shift out of the mid-infrared band. More traditional near-infrared and optical diagnostics such as Brα and Hα may be detectable for the most luminous galaxies out to redshifts of 10 (Serabyn et al. 1999, Haiman & Loeb 1998).

The ISO-SWS and ISOPHOT observations of distant galaxies lacked the spatial resolution to distinguish any structure. Figure 8 shows an ISOCAM image of one of the nearest AGN, the powerful radio galaxy Centaurus A (Mirabel et al. 1999). The 7 μm continuum image beautifully reveals a ~1 kpc barred spiral of warm dust feeding material to the AGN. ISOCAM-CVF spectroscopy shows that the nuclear region is dominated by AGN activity whereas the disk has a spectrum typical of star-forming regions with strong PAH 7.7 μm emission. The higher spatial resolution on NGST will be essential to distinguish the different regions of activity in more distant galaxies.

Figure 7. Diagnostic diagram showing the extinction-corrected 25.9 μm [O IV]/12.8 μm [Ne II] line ratios as functions of the strengths of the 7.7 μm PAH feature. Starburst galaxies are marked as open triangles, ULIRGs as filled circles and AGNs as crossed triangles. The areas of the diagram dominated by star formation and by AGNs are indicated (Genzel et al. 1998).

4. Star formation

The formation of stars and planetary systems from molecular clouds is accompanied by tremendous changes in the physical conditions, with densitities ranging 10^4 to 10^{13} cm^{-3} and temperatures from 10 to 10,000 K. The continuum emission from dust and the abundances and excitation of the atoms and molecules respond to these changes, so that mid-infrared imaging and spectroscopy provide a wealth of information with which to unravel the physical evolution. Tracing the chemical composition of gas and dust through the various stages of the star formation process is important as well, since it provides the raw material from which planetary systems like our own are made (e.g., van Dishoeck & Blake 1998, Langer et al. 2000). An overview of ISO spectroscopy of young stellar objects (YSOs) is given in van Dishoeck et al. (1999).

4.1. Cold pre-stellar cores

In the cold quiescent clouds prior to star formation, gas-phase molecules collide with the grains and stick, forming icy mantles around the silicate cores. Indeed, this freeze-out is predicted to be so efficient that it has been a puzzle for decades why any gas-phase molecules are seen at all in cold regions. Recent indirect evidence based on near-infrared star counts and millimeter data suggests that the amount of depletion inside dense cores can be substantial, with more than 90% of the heavy elements (including oxygen and carbon) frozen out onto the grains (Lada et al. 1999, Kramer et al. 1999). NGST will be the first instrument capable of probing this depletion process directly, through near- and mid-infrared observations of solid-state absorption bands towards hundreds of background

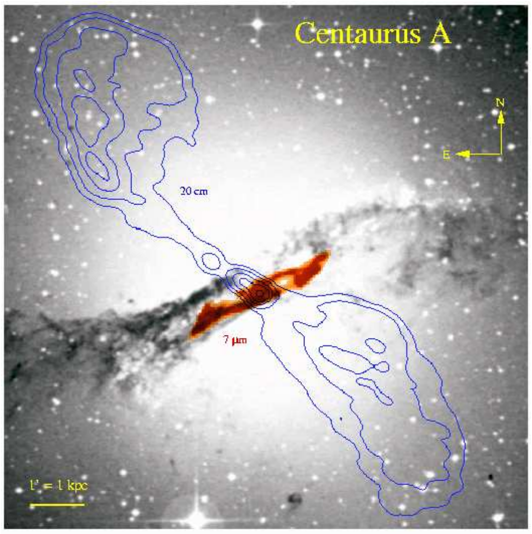

Figure 8. ISOCAM 7 μm image (dark image in center) and 20 cm continuum contours superposed on an optical image of Centaurus A (Mirabel et al. 1999).

stars located behind dark clouds, providing "maps" of the freeze-out process. Ground-based telescopes and SOFIA do not have enough sensitivity except for a few of the brightest stars, whereas SIRTF lacks spectral capabilities in the crucial 4–10 μm range.

4.2. Deeply embedded protostars

Mid-infrared observations on NGST will be particularly powerful to provide insight into the physical processes occurring in the deeply embedded protostellar phase when the star is still being assembled through accretion of material from the circumstellar disk. Mid-infrared continuum images at >20 μm probe the warm part of the accretion disk and the inner envelope, leading to constraints on the elusive mass infall rate (see simulations in Serabyn et al. 1999). Imaging in different spectral features such as the H_2 pure rotational lines and the [S I] 25.2 μm line probe the physics of the accretion shock at the disk surface, as well as the interaction of the outflow with the inner envelope as it starts to clear the surroundings (van den Ancker et al. 2000). The high sensitivity and spatial resolution of NGST are essential, since the youngest protostars have continuum fluxes of less than a mJy and the disks have sizes of only a few arcsec.

More distant, massive protostars are interesting targets for NGST mid-infrared observations as well. Little is known about the earliest stages of massive star formation, e.g., whether they are accompanied by circumstellar disks as in the case of low-mass star formation. Mid-infrared imaging at subarcsec resolution, combined with high resolution data on outflows from ALMA, can reveal such structures directly (e.g., Stecklum et al. 1998).

The ices in the cold outer envelope can be observed through medium-resolution absorption data toward the protostars themselves. In the earliest

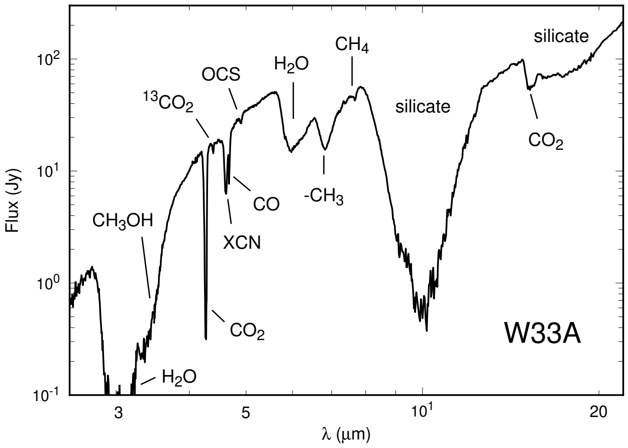

Figure 9. ISO-SWS spectrum of the deeply embedded massive YSO W 33A. A variety of ice mantle and refractory grain core features (silicates) are evident (Gibb et al. 2000).

stages, more than 99% of the heavy elements are predicted to be frozen out onto the grains, where the chemical composition is modified through grain-surface reactions. As the surroudings are heated by the protostar, the ices gradually evaporate back into the gas phase (Figure 4). Figure 9 shows the ISO-SWS mid-infrared spectrum toward the embedded massive YSO W 33A, which is particularly rich in various (organic) features. ISO has been able to obtain such high-quality spectra for only a dozen massive YSOs with luminosities of 10^3-10^5 $L_\odot$, but information on low-mass YSOs is lacking almost entirely. Only NGST will be able to perform a complete census of solid-state material as it enters the planet-forming disks around solar-type stars.

In addition to obtaining the overall solid-state composition, the ice and gas-phase data can reveal the thermal and irradiation history of the protostellar envelope. The solid CO_2 bending mode at 15 μm is a particularly sensitive diagnostic of the ice environment, with a characteristic double-peaked structure appearing at 15.15 and 15.25 μm upon heating (Gerakines et al. 1999). The systematic evolution of the profile with increasing temperature is a direct measure of the amount of thermal processing. Other features, such as the OCN^- feature at 4.62 μm, are sensitive to UV irradiation. Together, they record the cumulative events experienced during the protostellar phase such as FU-Orionis-type outbursts related to disk accretion.

4.3. Low–mass YSOs, brown dwarfs, KBOs

Mid-infrared imaging will be very powerful to address several other fundamental questions in star formation. In particular, the combination of near- and mid-infrared imaging of embedded clusters can establish the low-mass end of the initial mass function and probe its origin. Only NGST will have sufficient spatial resolution, sensitivity and wavelength coverage to bridge the gap between the current limit of $\sim$0.1 $M_\odot$ objects and the regime of Jupiter-like planets with $\sim$0.001 $M_\odot$. Mid-infrared spectroscopy with NGST of field brown dwarfs found

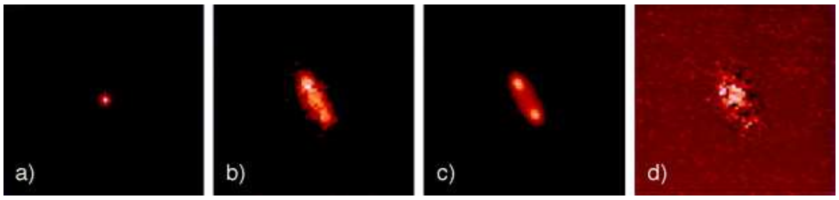

Figure 10. Mid-infrared imaging of the disk around the young star HR 4796A at 12.5 (a) and 20.8 μm (b) (Koerner et al. 1998). Note that the disk is seen only at long wavelengths. The two pictures on the right hand-side represent a model of a disk with a 55 AU inner hole (c) and the data minus model (d). This model has recently been confirmed through coronographic NICMOS imaging of the scattered light by Schneider et al. (1999).

by 2-μm all-sky surveys (2MASS, DENIS) and by SIRTF will be important to characterize their atmospheres. Finally, mid-infrared observations of outer solar-system objects such as Kuiper-Belt objects (KBOs) are essential to constrain their albedos and sizes.

5. Protoplanetary disks

One of the most exciting developments in astrophysics in the last decade has been the detection and imaging of circumstellar disks around young stars through infrared and millimeter observations (see Beckwith & Sargent 1996 for a review). Beautiful HST optical images of proplyds show such disks as silhouettes against the ionized background (e.g., McCaughrean & O'Dell 1996, Burrows et al. 1996), whereas NICMOS imaging at near-infrared wavelengths has revealed disks around young stars in the embedded stage (e.g., Padgett et al. 1999). The sizes of these disks are typically a few hundred AU, comparable to the size of our own primitive solar nebula. Around more mature stars, mid-infrared and submillimeter emission from debris disks has been detected, revealing holes, gaps and asymmetries (e.g., Koerner et al. 1998, Holland et al. 1998, Greaves et al. 1998) (see Figure 10). In these disks most of the original gas and dust has been dissipated and/or coagulated into larger bodies, but a small amount of dust is locally produced by collisions of planetesimals.

Optical and near-infrared images of disks are impressive, but they can only be observed under special conditions and provide little information about the physical parameters, such as their mass, their temperature and density structure, and their chemical composition. Observations of thermal emission at longer wavelengths are needed to probe these parameters. ALMA will be well suited to observe the cold gas and amorphous dust in the outer part of disks, and to study the kinematics through high-spectral resolution molecular data. Complementary mid-infrared observations with NGST are needed to probe the dust and gas in the warmer, inner planet-forming part of the disks and determine the solid-state composition.

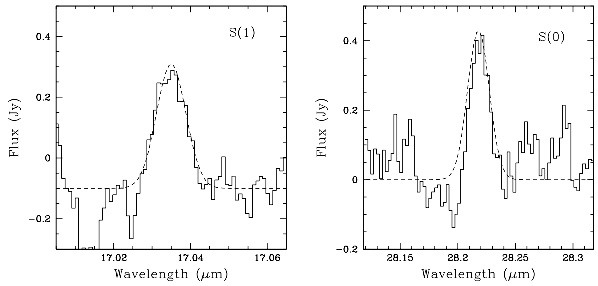

Figure 11. ISO–SWS spectra of the H_2 S(0) and S(1) lines toward the isolated T Tauri object GG Tau. This double-binary system is surrounded by a circumstellar dust and gas disk with a size of $\sim$800 AU. The H_2 lines provide direct information on the temperature and amount of warm gas (Thi et al. 1999).

The combination of NGST and ALMA data is essential to address several fundamental questions in the evolution of protoplanetary disks. For example, when does the transition from the massive, gas-rich disks seen around T Tauri stars (age $\sim 10^6$ yr, mass $\sim 10^{-2}$ $M_\odot$) to the debris disks seen around main sequence stars ($> 10^8$ yr, $< 10^{-8}$ $M_\odot$) occur? When does the gas disappear? How is this related to the settling of dust to the mid-plane and the coagulation of grains into planetesimals? When and where does crystallization occur? When do the gas-rich Jupiter-type planets form, and are they indeed responsible for the opening of gaps in the disks? What are the types of dust produced by collisions of planetesimals resulting in the debris disks, and how do they influence potential terrestrial planet formation? Finally, can we see evidence for the heavy bombardment stage in the final phase of planetary formation?

Potential key programs on NGST include a deep search for the H_2 28.2 μm S(0) and 17 μm S(1) lines in circumstellar disks to constrain their temperature structure, gas mass and gas/dust ratio (Figure 11). H_2 is the dominant molecule in disks and it does not suffer from freeze-out onto grains, in contrast with CO. NGST will be sensitive to gas with masses of $10^{-3} - 10^{-7}$ $M_\odot$ at $T_{\rm gas}$=50–200 K (see Figure 12). Such data will give constraints on the timescale for gas dissipation and are essential to test theories of gas-rich giant planet formation.

Another key program will be an imaging survey of hundreds of disks in the solar neighborhood, which will provide information on the structure of the disks (gaps, asymmetries). Spatially resolved imaging spectroscopy (long-slit or integral field) will reveal the solid-state composition as a function of position and age. Together, such data will greatly strengthen our understanding of the relation between disks and solar system material (Figure 13).

6. Late-type stars, supernovae and supernovae remnants

Late-type stars and supernovae will also be excellent targets for mid-infrared instrumentation on NGST. In the last phases of their lives, stars of moderate mass begin to pulsate and lose their outer layers. The ejected material is enriched in elements formed by nucleosynthesis inside stars. In the cooling outflow, solid particles such as silicates, oxides and carbonaceous material can condense,

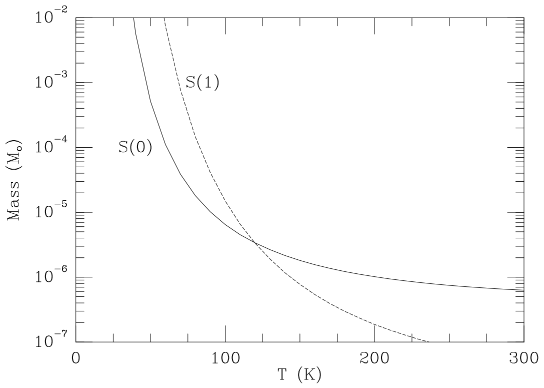

Figure 12. Limiting mass of warm gas per square arcsec (∼1 resolution element at 28 μm) as a function of temperature that can be detected with NGST from a source at a distance of 140 pc, assuming a flux limit of 1 mJy at R=3000. Note that the S(0) line is up to three orders of magnitude more sensitive than the S(1) line at $T < 100$, and that both lines are needed to constrain the temperature and mass.

resulting in very rich mid-infrared spectra (e.g., Waters et al. 1999, Molster et al. 1999). NGST will be able to trace the formation of dust through spatially resolved imaging of spectral features in nearby objects, and through spectroscopy of much more distant objects, both in our own galaxy and in external galaxies with different metallicities well beyond the local group.

Supernovae end their lives through a spectacular explosion, expelling many heavy elements. NGST will have the sensitivity and spatial resolution to observe the in-situ formation of dust in knots with greatly different elemental abundances.

Finally, NGST can be used to trace the interaction of supernovae remnants with the interstellar medium. Figure 14 shows ISOCAM-CVF images of the supernova remnant IC 443. Surprisingly, no dust continuum is seen, but all the broad-band emission as seen, for example, by IRAS is found to be due to line emission, in particular H_2 at 12 and 28 μm. The H_2 lines measure directly the temperature structure of the shock and thereby test the physical models.

In summary, the enormous increase in sensitivity and spatial resolution of NGST at mid-infrared wavelengths compared with other facilities will allow many fundamental questions in modern astrophysics to be addressed. In addition, it provides the opportunity for unexpected, new avenues of science that have not yet even been considered. A mid-infrared camera *and* spectrometer on NGST will be an essential observational tool to study the universe and our origins in the coming decades.

Acknowledgments

The author is grateful to many colleagues, in particular M. Barsony, A. Blain, A. Boogert, A. Burrows, P. Cox, Th. de Graauw, C. Dominik, D. Elbaz, A. Ferrara, A. Francescini, J. Graham, T. Greene, Th. Henning, D. Koerner, O. Laurent, D. Lutz, L. Metcalfe, M. Meyer, F. Mirabel, M. Rieke, E. Serabyn,

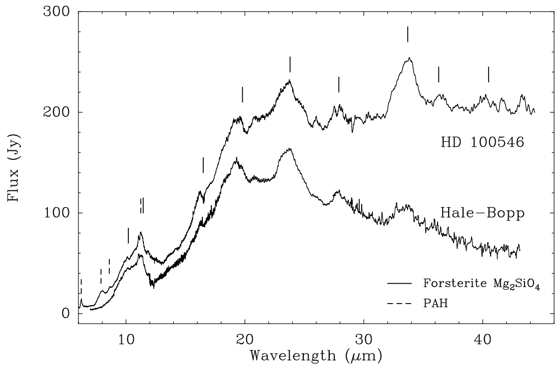

Figure 13. ISO-SWS spectrum of the circumstellar disk around the young Herbig Ae star HD 100546, showing spectral features due to crystalline forsterite (Mg_2SiO_4) and PAHs (Waelkens et al. 1996, Malfait et al. 1998). For comparison, the ISO-SWS spectrum toward comet Hale-Bopp is shown as well (Crovisier et al. 1997). Note the remarkable similarity in composition between the circumstellar and solar-system material.

P. Stockman, W.-F. Thi, X. Tielens, P. van der Werf, C. Waelkens, R. Waters, D. Whittet, and G. Wright, for many stimulating discussions and for providing input and figures for the mid-infrared science case with NGST.

References

Altieri, B., Metcalfe, L., Kneib, J-P., et al. 1999, A&A, 343, L65

Beckwith, S.V.W., Sargent, A.I. 1996, Nature, 383, 139

Bertoldi, F., Timmermann, R., Rosenthal, D., Drapatz, S., Wright, C.M. 1999, A&A, 346, 267

Blain, A.W., Kneib, J.-P., Ivison, R.J., Smail, I. 1999, ApJ, 512, L87

Boogert, A.C.A. 1999, PhD Thesis, Univ. of Groningen

Burrows, A., Marley, M., Hubbard, W.B., et al. 1997, ApJ, 491, 856

Burrows, C.J., Stapelfeldt, K.R., Watson, A.M. et al. 1996, ApJ, 473, 437

Cesarsky, D., Cox, P., Boulanger, F., van Dishoeck, E.F., Wright, C.M. 1999, A&A, 348, 945

Cox, P., Kessler, M.F., eds. 1999, The Universe as seen by ISO, ESA SP-427 (Noordwijk: ESTEC)

Crovisier, J., Leech, K., Bockelée-Morvan, D., et al. 1997, Science, 275, 1904

Draine, B.T., Bertoldi, F. 1999, in 'The Universe as seen by ISO', ESA SP-427, p. 553

Elbaz, D., Cesarsky, C.J., Fadda, D., et al. 1999, A&A, in press

Genzel, R., Lutz, D., Sturm, E., et al. 1998, ApJ, 498, 579

Gerakines, P.A., Whittet, D.C.B., Ehrenfreund, P., et al. 1999, ApJ, 522, 357

Gibb, E., Whittet, D.C.B., Gerakines, P., et al. 2000, ApJ, submitted

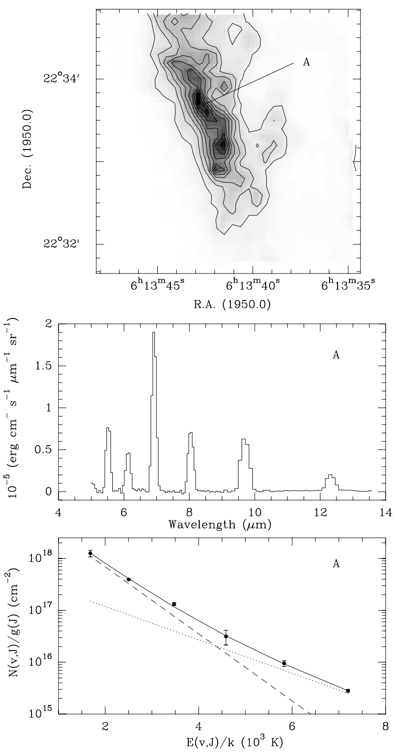

Figure 14. ISOCAM-CVF spectro-imaging of the supernova remnant IC 443 (clump G) (Cesarsky et al. 1999). Top: distribution of emission in the H_2 S(2) to S(7) lines. Middle: spectrum toward the emission peak A; Bottom: H_2 excitation diagram at position A. The lines indicate the best fit with a two-component model, with $T_{\rm hot} \approx 1200$ K and $T_{\rm warm} \approx 500$ K. The S(0) and S(1) lines have not been observed toward IC 443, but often indicate a colder component with $T \approx 100$ K in other sources.

Greaves, J.S., Holland, W.S., Moriarty-Schieven, G., et al. 1998, ApJ, 506, L133

Haiman, Z., Loeb, A. 1998, ApJ, 503, 505

Holland, W.S., Greaves, J.S., Zuckerman, B., et al. 1998, Nature, 392, 788

Hughes, D.H., Serjeant, S., Dunlop, J., et al. 1998, Nature, 394, 241

Koerner, D.W., Ressler, M.E., Werner, M.W., Backman, D.E. 1998, ApJ, 505, 358

Kramer, C., Alves, J., Lada, C.J., et al. 1999, A&A, 342, 257

Lada, C.J., Alves, J., Lada, E.A. 1999, ApJ, 512, L250

Langer, W.D., van Dishoeck, E.F., Blake, G.A., Bergin, E., Tielens, A.G.G.M., Velusamy, T., Whittet, D.C.B. 2000, Protostars & Planets IV, eds. V. Mannings, A. Boss, S. Russell (Tucson: Univ. of Arizona), in press

Laurent, O., Mirabel, I.F., Charmandaris, V., Gallais, P., Vigroux, L., Cesarsky, C.J. 1999, in 'The Universe as seen by ISO', ESA-SP 427, p. 913

Lutz, D., Spoon, H.W.W., Rigopoulou, D., Moorwood, A.F.M., Genzel, R. 1998, ApJ, 505, L103

Malfait, K., Waelkens, C., Waters, L.B.F.M., Vandenbussche, B., Huygen, E., de Graauw, Th., 1998, A&A, 332, L25

McCaughrean, M.J., O'Dell, C.R. 1996, AJ, 111, 1977

Metcalfe, L., Altieri, B., McBreen, B., et al. 1999, in 'The Universe as seen by ISO', ESA SP-427, p. 1019

Mirabel, I.F., Laurent, O., Sanders, D.B. et al. 1999, A&A, 341, 667

Molster, F.J., Waters, L.B.F.M., Trams, N.R., et al. 1999, A&A, 350, 163

Padgett, D.L., Brandner, W., Stapelfeldt, K.R., Strom, S.E., Terebey, S., Koerner, D. 1999, AJ, 117, 1490

Serabyn, E., et al. 1999, A mid-infrared camera for NGST, `http://www.ngst.nasa.gov/science/isimpage.html`

Smail, I., Ivison, R.J., Blain, A.W. 1997, ApJ, 490, L5

Schneider, G., Smith, B.A., Becklin, E.E., et al. 1999, ApJ, 513, L127

Stecklum, B., Henning, T., Feldt, M., Hayward, T.L., Hoare, M.G., Hofner, P., Richter, S. 1998, AJ, 115, 767

Thi, W.F., van Dishoeck, E.F., Blake, G.A., van Zadelhoff, G.J., Hogerheijde, M.R. 1999, ApJ, 521, L63

Tielens, A.G.G.M., Hony, S., van Kerckhoven, C., Peeters, E. 1999, in 'The Universe as seen by ISO', ESA SP-427, p. 579

van den Ancker, M.E., Tielens, A.G.G.M., Wesselius, P.R. 2000, A&A, to be submitted

van Dishoeck, E.F., Blake, G.A. 1998, ARAA, 36, 317

van Dishoeck, E.F., Wright, C.M., Cernicharo, J., González-Alfonso, E., Helmich, F.P., de Graauw, Th., Vandenbussche, B. 1998, ApJ, 502, L173

van Dishoeck, E.F., Black, J.H., Blake, G.A., et al. 1999, in 'The Universe as seen by ISO', ESA SP-427, p. 437

Vigroux, L., Mirabel, F., Altieri, B. et al. 1996, A&A, 315, L93

Waelkens, C., Waters, L.B.F.M., de Graauw, Th., et al. 1996, A&A, 315, L245

Waters, L.B.F.M., Beintema, D.A., Cami, J., et al. 1999, in 'The Universe as seen by ISO', ESA SP-427, p. 219

Waters, L.B.F.M., Molster, F.J., de Jong, T., et al. 1996, A&A, 315, L361

Wright, C.M. 2000, in 'Astrochemistry: from Molecular Clouds to Planetary Systems', eds. Y.C. Minh & E.F. van Dishoeck, IAU Symposium 197 (ASP), in press

Wright, C.M., van Dishoeck, E.F., Cox, P., Sidher, S.D., Kessler, M.F. 1999, ApJ, 515, L29

Wright, G., et al. 1999, MIRCAM and MIRIFS, `http://www.ngst.nasa.gov/science/isimpage.html`